Available online at www.sciencedirect.com

SciVerse ScienceDirect

Procedia IUTAM 4 (2012) 133 – 143

Procedia IUTAM

www.elsevier.com/locate/procedia

Full field measurements and identification in Solid Mechanics

Combining Laue microdiffraction and digital image correlation for improved measurements of the elastic strain field with micrometer spatial resolution

J. Petit[a], M. Bornert[b], F. Hofmann[g], O. Robach[c,e], J.S. Micha[d,e], O. Ulrich[c,e], C. Le Bourlot[a,f], D. Faurie[f], A.M. Korsunsky[g], O. Castelnau[a*]

[a]*PIMM, CNRS, 151 Bd de l'Hôpital, 75013 Paris*
[b]*Laboratoire NAVIER, Université Paris-Est, École des ponts ParisTech, 77455 Marne-la-Vallée, France*
[c]*CEA-Grenoble, INAC/SP2M/NRS, 17 rue des Martyrs, 38054 Grenoble Cedex 9, France*
[d]*UMR SPrAM CNRS-CEA-UJF, CEA-Grenoble, INAC, 17 rue des Martyrs, 38054 Grenoble Cedex 9,France*
[e]*CEA-CNRS CRG-IF BM32 beamline at ESRF, 6 rue Jules Horowitz, 38043 Grenoble Cedex 9,France*
[f]*LSPM, CNRS, Université Paris 13, 93430 Villetaneuse, France*
[g]*Department of Engineering Science, University of Oxford, Parks Road, Oxford OX1 3PJ, UK*

Abstract

The X-ray Laue microdiffraction technique, available at beamline BM32 on the synchrotron ESRF, is ideally suited for probing the field of elastic strain (and associated stress) in deformed polycrystalline materials with a micrometric spatial resolution. We show that using Digital Image Correlation for measuring Laue pattern distortions between two mechanical states improves significantly the estimate of elastic strain increment. The potentiality of this new Laue-DIC method is illustrated on an elastically bent Si single crystal, for which the measured elastic strain deviates not more than 10^{-5} from the theoretical strain distribution provided by standard solutions.

Keywords: X-ray Laue microdiffraction; Digital Images Correlation (DIC); stress field; four point bending; microscopic analysis

1. Introduction

The use of diffraction techniques for stress field analysis (through the measurement of the associated elastic strain) is increasingly widespread thanks to the possibility of in-situ and non-destructive

* Corresponding author. Tel.: +03317196555; fax: +033171936555.
E-mail address: olivier.castelnau@ensam.eu

2210-9838
doi:10.1016/j.piutam.2012.05.015

measurements. Most X-ray diffractometers enable measurements at the macroscopic scale (0.1-10mm). With the increasing need from industry to develop materials of high mechanical performance, a good understanding of their properties at the mesoscale (0.1-10µm) has become critical since many of these properties are responsible for the macroscopic mechanical behaviour. Third generation synchrotron radiation facilities [1,2], such as the ESRF in Grenoble (France) [3], are able to produce intense X-ray beams with sub-micrometer cross section. White (*i.e.* broadband polychromatic) X-ray microdiffraction makes it possible to distinguish the diffraction patterns related to different grains (or subgrains) with a typical probe volume of the order of few μm^3 inside a polycrystal. Important applications use this technique to identify phase and strain with submicrometer spatial resolution [4-6]. X-ray microdiffraction is a particularly exciting application compared with alternative probes of crystalline phase, orientation, and strain, as it offers better strain resolution, competitive or superior spatial resolution in thick samples, and the ability to probe below the sample surface.

When the cross section of the white X-ray beam is smaller than the grain size, a single Laue diffraction pattern is recorded on the 2-D detector. The elastic strain can then be deduced from the position of Laue spots on the detector. Specific softwares (*e.g.* XMAS and LaueTools) have been developed for that purpose [7 –10]. They are based on algorithms allowing the rapid indexation of white-beam Laue spots and calculation of the orientation-strain matrix related to local lattice parameters. In spite of the quality of these analysis routines, errors may be introduced in the determination of the Laue spots position since the Gaussian- or Pearson-type functions used for fitting the Laue spots are often not appropriate. Moreover, the evaluation of the spot position strongly depends on geometrical features of the experimental setup which must be known to a high accuracy. Consequently, uncertainties on the orientation-strain matrix are often too large [11] to allow their use for micromechanical studies.

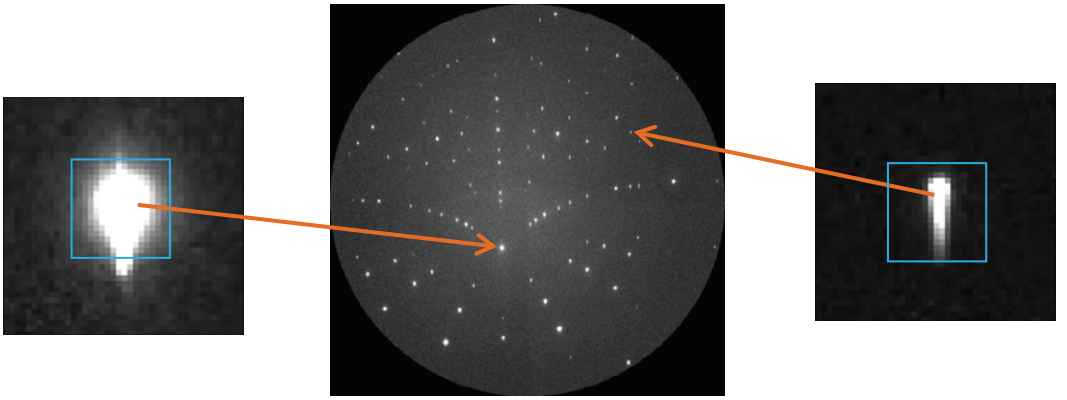

Fig. 1. Typical Laue pattern obtained on a Si single crystal. The blue squares represent the zone of interest (ZOI) around Laue spots (zoom) used for DIC.

This work aims to develop a new method (denoted Laue-DIC) for minimizing errors due to geometrical setup uncertainties and improving the accuracy on elastic strains determination. The displacement of each Laue spot is directly investigated without the requirement to determine its position accurately. This is realized by applying the Digital Image Correlation (DIC) technique [12] to Laue patterns recorded for successive positions of the probe volume on an inhomogeneously deformed specimen. To illustrate the potentiality of the method, we consider the case of a Si single crystal deformed under four point bending. Elastic strain profiles across the specimen are obtained at a given loading step by performing a line-scan across the sample surface with the white micro-beam, with micrometer spatial resolution, recording a

Laue pattern at each beam position. The deviatoric stress tensor is calculated using the anisotropic elastic stiffness of the material.

2. Experiments

2.1. Instrumental considerations

The usual way of performing X-ray diffraction is to set the photon energy (inversely proportional to the wavelength λ) and map the Bragg reflection peaks by rotating the sample while detecting the diffracted X-rays with a detector. Using Bragg law, $\lambda = 2\, d_{hkl} \sin\theta$ with θ the scattering angle, allows estimating the mean lattice spacing d_{hkl} of the diffracting planes with Miller indices (*hkl*). Although some results *e.g.* on dislocation structure and associated stored energy could be evaluated by this technique [13, 14], it is inappropriate for spatial resolution as fine as a micrometer since current high-quality diffractometers exhibit a sphere of confusion (*i.e.* the distance between all needed rotation axes) of a few tens of µm at best, and thus any rotation would move the point of interest of the sample out of the micro-beam.

With the microdiffraction setup available at beamline BM32 of the European synchrotron ESRF, the sample does not need to be rotated thanks to the use of a white beam, and thus the spatial resolution is only limited by the beam size. The beam position being constant (and very stable), translation motions of the sample are performed in order to get a map of elastic strain. The associated stress map can be calculated if the local elastic behaviour is known. For each sample position, the diffracted X-rays are recorded on a CCD detector as a Laue diffraction pattern, such as shown in figure 1. The MAR detector is made up of a scintillator linked to a CCD sensor by a single fiber-optic taper and the demagnification ratio is 2.7:1. The CCD is a 4096 x 4096 pixels binned 2 x 2 sensor with an original pixel size of 80.6µm and a saturation level of 360000 electrons for 12keV photons, leading to a signal-to-photon-noise ratio of about 600 at saturation. Typical exposure time is 0.5s and images are digitized with a 16-bit A/D converter with a readout time of about 5s.

A typical Laue image is shown in figure 1. It consists of over a hundred Laue spots with an elongated shape due the penetration of X-rays into the thick Si crystal. The higher the spot intensity, the broader the spot becomes and the more closely the top of the spot approaches a Gaussian shape. But, none of them can really be fitted by simple analytical functions such as Gaussian. The rest of the image is formed by the background-noise due to the random diffusion of the photons, and fluorescence scattering. The background is very lightly domed from the centre of the image to the detector periphery.

2.2. Setup and calibration

Four point bending tests were carried out on a Si single crystal bar of length 10mm (figure 2). The width of the bar (along *x*-direction) was 1.820mm with a greatest deviation of ±1µm over the 10mm length. The thickness of the bar (*z*-direction) varied linearly from 0.671mm at one end to 0.683mm at the other. The crystal was oriented so that direction [101] was approximately aligned with the sample *x*-axis, $[12\bar{1}]$ with the *y*-axis, and $[\bar{1}11]$ with the *z*-axis. Flatness of all faces was better than 1µm and the surfaces were polished to a mirror finish with negligible roughness.

Loading was applied according to the schematic diagram in figure 2. The distance between loading pins A and D was 8mm, and distance between B and C was 3mm. Laue patterns were recorded along a line parallel to the *x*-direction and centred between pins B and C.

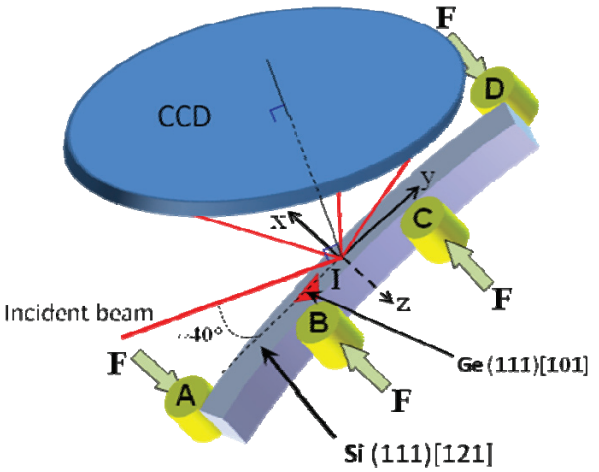

Fig. 2. Schematic sample arrangement for the micro-beam Laue four point bending measurements. Ge is used to determine the setup calibration. The sample is scanned along direction *x*, and at each position, a Laue pattern is recorded on the CCD. *y* is along the specimen longitudinal direction, and *z* along the transverse direction.

At the beginning and the end of each loading step and Laue measurements, calibration patterns were collected on a Ge single crystal positioned next to the scanned line. Laue spots are very small and sharp, and therefore these patterns allow the accurate determination of all geometrical parameters of the experimental setup such as the detector to sample distance, the detector orientation, etc. The four point bending configuration is suitable for the study of the tensile and compressive material response. In the central area of the sample (between pins B and C), pure bending moment loading is expected. Kinematics and elasticity theory prescribe that strain varies linearly along the transverse *x*-direction. The sample was loaded incrementally; here, we report results obtained for two load levels, 0N and 50N.

3. Problem formulation

Let's consider two configurations (or deformation states) for the specimen, a reference one and a deformed one. Hereafter, the two configurations will correspond to two different positions on the heterogeneously deformed crystal. Let's also build matrices whose columns are the components of the three lattice vectors **a**, **b**, **c** of the crystal, expressed in an orthonormal reference frame. We denote in the following $\underline{\underline{M}}_0$ the matrix corresponding to the reference configuration, and $\underline{\underline{M}}$' that for the deformed configuration. Since we are considering only elastic strains, *i.e.* small strains, the elastic strain tensor $\underline{\underline{\varepsilon}}$ is given by

$$\underline{\underline{\varepsilon}} = \frac{{}^{t}\underline{\underline{F}} + \underline{\underline{F}}}{2} - \underline{\underline{I}} \qquad (1)$$

with $\underline{\underline{I}}$ the identity tensor and $\underline{\underline{F}}$ the mechanical deformation gradient between both configurations

$$\underline{\underline{F}} = \underline{\underline{I}} + \underline{\underline{\varepsilon}} + \underline{\underline{\omega}} = \begin{pmatrix} 1+\varepsilon_{xx} & \varepsilon_{xy}+\omega_{xy} & \varepsilon_{xz}+\omega_{xz} \\ \varepsilon_{xy}-\omega_{xy} & 1+\varepsilon_{yy} & \varepsilon_{yz}+\omega_{yz} \\ \varepsilon_{xy}-\omega_{xz} & \varepsilon_{yz}-\omega_{yz} & 1+\varepsilon_{zz} \end{pmatrix} \quad (2)$$

with $\underline{\underline{\omega}}$ the rotation tensor. In the general case, $\underline{\underline{F}}$ has 9 independent components. Matrices M_0 and M' are linked by the following relation

$$\underline{\underline{M}}' = \underline{\underline{F}} \bullet \underline{\underline{M}}_0 . \quad (3)$$

Let's also define a geometrical function f that relates the position of a given Laue spot on the detector (*i.e.* the spot coordinates in a given reference frame) to the Miller indices (hkl) of the corresponding diffracting plane. Denoting X_{hkl} the Laue spot coordinates for the reference configuration and X'_{hkl} the ones for the deformed configuration, we have

$$X_{hkl} = f(\underline{\underline{M}}_0, \{h,k,l\}) , \qquad X'_{hkl} = f(\underline{\underline{M}}', \{h,k,l\}) . \quad (4)$$

Here, function f accounts for the complete geometrical arrangement of the setup (sample to detector distance, detector orientation, etc.).

3.1. The standard procedure for Laue microdiffraction

The standard procedure classically used for the estimation of elastic strain from Laue patterns runs as follows. First, function f is identified with a well known and strain free specimen, such as a Ge single crystal. Next, positions X'_{hkl} are measured for the specimen of interest and relation (4b) is inverted to find $\underline{\underline{M}}'$. Finally, the deformation gradient $\underline{\underline{F}}$ is evaluated with relation (3) in which the undeformed lattice parameters are usually taken from the literature. Three main sources of uncertainties thus arise:

(i) Positions X'_{hkl} are determined by fitting the Laue spots with Gaussian- or Pearson-type functions. As illustrated in figure 1, such functions are not appropriate in many cases.

(ii) The function f is obtained by minimizing an error function (in a Linear Least-Square Minimization sense) associated to the distance between the measured positions X_{hkl} of Laue spots on the detector for the Ge crystal with the computed ones $f(\underline{\underline{M}}_{Ge}, \{h,k,l\})$, for all ($hkl$) reflections. Again, the measured positions are obtained by a Gaussian- or Pearson-type fitting, leading to errors on f, that are also sensitive to distortions of the detector grid.

(iii) $\underline{\underline{M}}_0$ and $\underline{\underline{M}}'$ are determined independently. Both matrices integrate the errors defined in (i) and (ii). So, when comparing the deformed state $\underline{\underline{M}}'$ with the reference one $\underline{\underline{M}}_0$, errors on the geometrical calibration of the setup, that are included in the definition of f, are counted twice.

Hence, important uncertainties can arise in the determination of $\underline{\underline{\varepsilon}}$.

3.2. The new Laue-DIC method

With the new approach proposed in this paper, we are not looking for the absolute position X_{hkl} of Laue spots, but we are only characterizing precisely their *displacement* X'_{hkl} - X_{hkl}. This is done by using a Digital Image Correlation (DIC) technique between the two Laue patterns corresponding to the reference and the deformed configurations. Hence the Laue-DIC method. Moreover, we consider the first order expansion for the function f, which is a valid approximation since only (small) elastic strain are determined by diffraction techniques (and therefore small displacements of Laue spots on the detector). Denoting $\underline{\underline{dM}} = \underline{\underline{M}}' - \underline{\underline{M}}_0$, one obtains

$$\begin{aligned} X'_{hkl} - X_{hkl} &= f(\underline{\underline{M}}', \{h,k,l\}) - f(\underline{\underline{M}}_0, \{h,k,l\}) \\ &= f([\underline{\underline{M}}_0 + \underline{\underline{dM}}], \{h,k,l\}) - f(\underline{\underline{M}}_0, \{h,k,l\}) \\ &\approx \frac{\partial f}{\partial \underline{\underline{M}}}(\underline{\underline{M}}_0, \{h,k,l\}) \,.\, \underline{\underline{dM}}. \end{aligned} \quad (5)$$

Therefore, the increment of crystal lattice between configurations $\underline{\underline{M}}_0$ and $\underline{\underline{M}}'$ is given by

$$\underline{\underline{dM}} = \left(\frac{\partial f}{\partial \underline{\underline{M}}} \left(\underline{\underline{M}}_0, \{h,k,l\} \right) \right)^{-1} . (X'_{hkl} - X_{hkl}) \quad (6)$$

and the transformation gradient by

$$\underline{\underline{F}} = I + \underline{\underline{dM}}.\underline{\underline{M}}_0^{-1}. \quad (7)$$

Doing so, uncertainties on $\underline{\underline{\varepsilon}}$ can be significantly reduced compared to the standard procedure, since $X'_{hkl} - X_{hkl}$ can be determined with much higher accuracy with DIC (described hereafter) than with the fitting procedure described above. Moreover, one do not need to know very precisely the *absolute* spot positions X_{hkl}, subjected *e.g.* to errors due to grid distortion of the detector, but only their *relative* motion. And finally, it can be checked that the gradient $\frac{\partial f}{\partial \underline{\underline{M}}}\left(\underline{\underline{M}}_0, \{h,k,l\} \right)$ is much less sensitive to variations of $\underline{\underline{M}}_0$ than the function f itself.

4. Determination of spot displacement field by Digital Image Correlation (DIC)

4.1. DIC Background

DIC is a full-field measurement technique developed at the beginning of the 1980s [15, 16]. The method consists in matching a speckled pattern in similar images taken before and after displacement, providing thus the displacement field of the speckle in the camera reference frame. The field can represent the physical displacement of the specimen surface when this gray level pattern is attached to the specimen surface [17] or, as in the present case the displacement of Laue spots (generated by the sample microstructure) on the detector area.

To determine a displacement field in a given image with respect to a reference image, one considers a set of sub-images that will be referred to as “Zone of Interest” (ZOI). In the following, every ZOI has the same size and is centred on one Laue spot (figure 1). The aim of DIC is to match the same ZOI in two images captured at different positions x. The displacement of the centre of a given ZOI between both images is the sought displacement. A correlation function, compatible with a possible variation of the brightness and the contrast of the grey level between the two images, is used to measure the similarity between the sub-images. Its optimization with respect to the components of the shape function linking the relative distortion between the two sub-images leads to a subpixel evaluation of the sought displacement. The in-house CorrelManuV DIC software developed at LMS and Navier [18] was used in this study to determine spot displacements. To evaluate sub-pixel displacements, the grey levels in the sub-images are interpolated by a bilinear function and simple translation is used as shape function. More sophisticated interpolations functions (bicubic or biquintic) did not improve the results for this experiment. DIC has been shown to provide, in different contexts, an accuracy of displacement of typically a few hundredths of pixels [15].

The CCD camera pixel number, the dynamic range of the sensor and the noise/signal ratio influence the quantity and the quality of information. In classical applications of DIC, spatial resolution strongly depends, amongst other things, on the choice of the size of the sub-images. In most DIC applications, a compromise between uncertainty and spatial resolution for mechanical displacement must be found for the sub-images size. For the Laue microdiffraction technique, spatial resolution is not related to the DIC measurements but to the beam size. So, the size of the sub-images was taken sufficiently large to encompass the whole spot, including its tail and the associated background. Besides, performances in terms of displacement and strain resolutions are often improved when there is a high dynamic range of the picture. In practice, when the sample surface is directly imaged on the camera sensor, an artificial texture with a random pattern is deposited on it. In the present case, speckle pattern of images cannot be changed. Various error regimes were identified in [18, 19], for which the dependence of the uncertainty with the speckle pattern and the parameters of the algorithms, such as sub-image size, gray level interpolation or shape functions, is discussed.

4.2. Image analysis

The evaluation of the deviatoric elastic strain tensor was performed from all Laue spots that could be indexed beforehand by the LaueTools [10] software. Some spots and particularly spots with low intensity are excluded from the fit. In this study we performed image correlation, for the two load levels, between the Laue pattern measured at a given position x and the reference pattern measured at the position of the neutral axis. The motion of Laue spots between these two images is characteristic of the distribution of elastic strain along the specimen width. As an example, figure 3 gives the spot displacement field between the neutral axis and position x=0.9mm. The X-ray micro-beam enters the sample surface ($z = 0$) halfway between the B and C bending pins ($y = 0$).

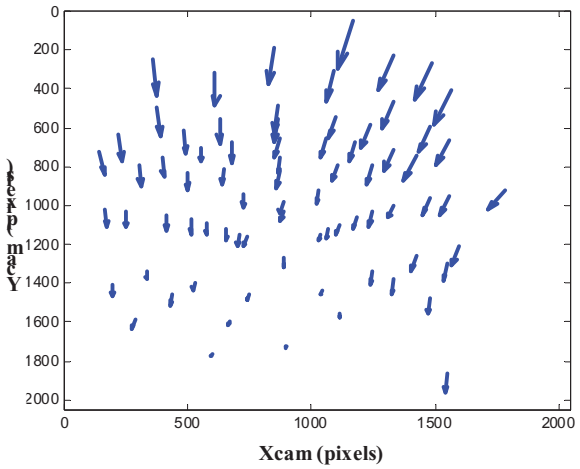

Fig. 3. Laue spot displacement field between the neutral fiber and an end fiber, obtained by digital image correlation. The scale of arrows is enlarged (by a factor 100). Here, the detector axis Xcam lies (approximately) parallel to the specimen loading direction, and Ycam is (approximately) parallel to the incident X-ray beam. Both Xcam and Ycam are given in pixel unit.

Displacement $X'_{hkl} - X_{hkl}$ of Laue spots can also be calculated using equations (1-7) for a given deformation gradient. The effects of the each component of the deviatoric elastic strain tensor on Laue pattern distortion is shown in figure 4. It can be observed that the experimental field shown in figure 3 is

very close to the theoretical field obtained when considering only ε^d_{yy}, *i.e.* an axial deviatoric elastic strain along the *y*-direction. This is consistent with the pure bending of the four point test, with an undeformed neutral axis. However, in the experimental measurements, all arrows point downwards contrarily to the sole effect of ε^d_{yy}. This can be due to transverse strains (ε^d_{xx} or ε^d_{zz}). Other spot motions due to a small shear and/or a small lattice rotation due to slight imperfections of the bending test could also superimpose to the dominant ε^d_{yy} strain. More spots appear in figure 4 than in figure 3, because theoretical patterns include all spots in the energy range of 5-22keV for the incoming beam, while low-intensity high Miller indices spots are filtered out from the list of experimental spots.

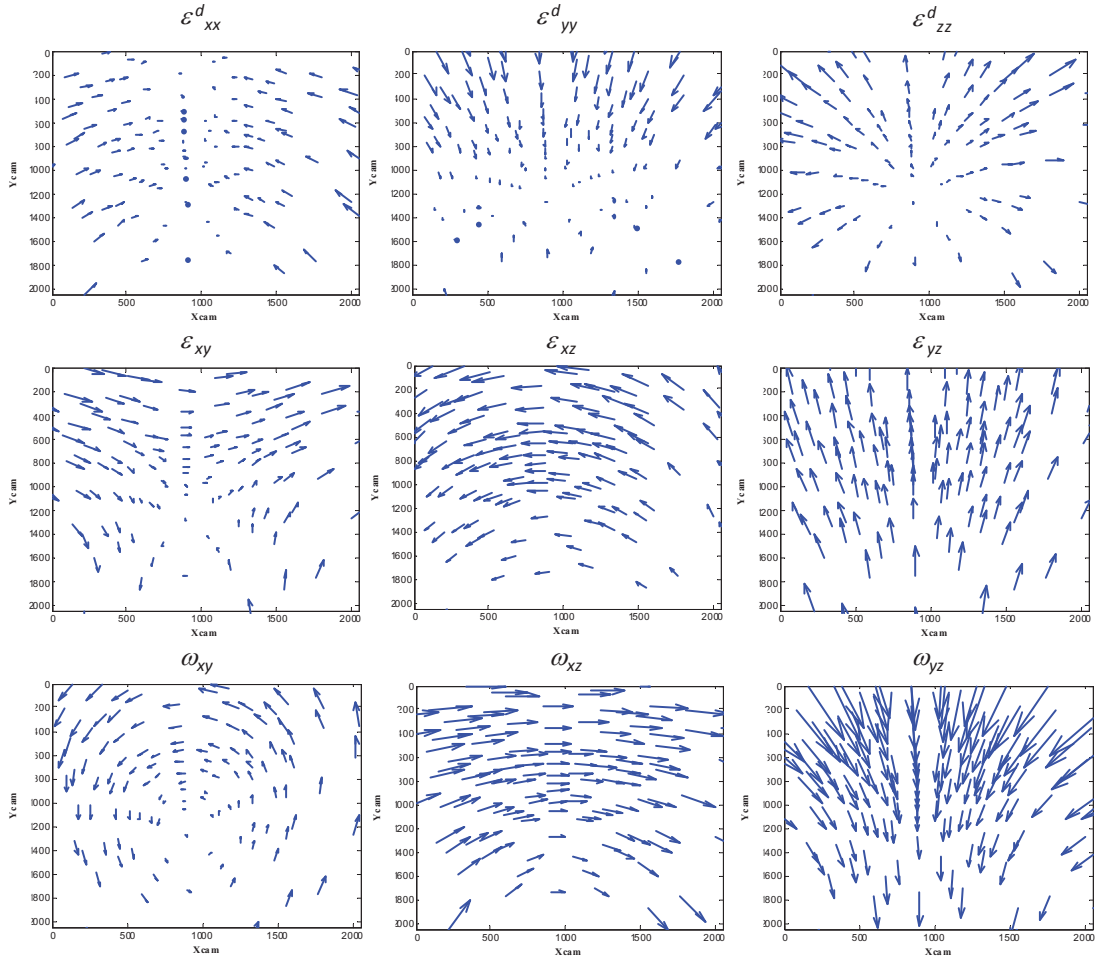

Fig. 4. Theoretical effect of each component of the deviatoric elastic strain tensor and the lattice rotations on the Laue spot displacement field of the Si sample considered during this experiment. Patterns are calculated for the standard setup available at beamline BM32 of the ESRF. Same detector orientation as in figure 3.

5. Distribution of elastic strain (and related stress) in a Si bar

Deviatoric stress was mapped with a micrometric spatial resolution along a line scan along *x* (step 20 µm) inside the bent Si single crystal. It was computed from the deviatoric elastic strain tensor obtained

by Laue-DIC combined with an identification method. This latter consists in finding, by a Linear Least-Square Minimization for all indexed spots, the 8 best independent components of the deviatoric part of $\underline{\underline{F}}$ which enable to transform $\underline{\underline{M}}_0$ into $\underline{\underline{M}}' = \underline{\underline{F}}.\underline{\underline{M}}_0$. The minimization was realized with a Levenberg-Marquardt's algorithm. The last component of $\underline{\underline{F}}$, which corresponds to the trace of the elastic strain tensor, cannot be directly determined by white beam Laue microdiffraction; it could be assessed by measuring the photon energy for one particular Laue beam.

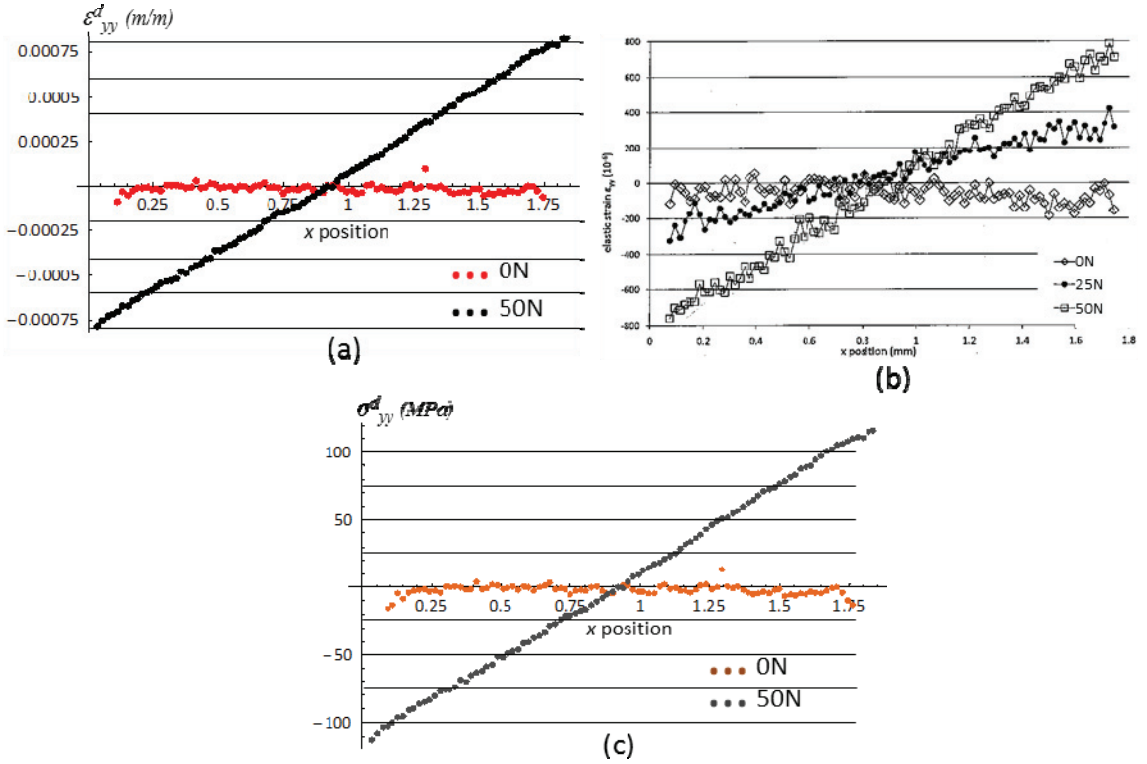

Fig 5. Deviatoric elastic strain ε^d_{yy} distribution obtained by (a) the new Laue-DIC approach and (b) the standard procedure [20]. (c) deviatoric stress σ^d_{yy} distribution derived from (a).

Figures 5(a) and 5(c) show the distribution of the measured deviatoric elastic strain ε^d_{yy} and the deviatoric stress σ^d_{yy} along the *x*-axis, for two loading states: 0N and 50N overall compression force on the bending setup. It can be observed that ε^d_{yy} and σ^d_{yy} are very close to a linear profile for 50N, as expected from the beam asymptotic theory and checked for the present geometry by Finite-Element simulation incorporating the anisotropic elastic behavior of the Si crystal and the boundary conditions for four point bending. The standard deviations of experimental results with respect to the expected linear stress distributions are given in Table 1 for the two loadings steps; uncertainties of only a few MPa are obtained, which is remarkable. From the experimental deviatoric stress profile σ^d_{yy}, it is also possible to estimate the applied load, knowing that $\sigma_{xx}=\sigma_{zz}=0$ along the *x*-axis at $y=0$. A value of 51.6N was obtained, *i.e.* a difference of only 3.2% with respect to the nominal load (50N). But note that the force during the bending test is measured with only a similar accuracy, and that the elastic constant for Si is also known with an accuracy of few % to the best of our knowledge.

Table 1. Standard deviations on elastic strain and stress distribution (with respect to the theoretical linear distribution), and load computed according to the measured profile of deviatoric stress.

Loading state *(N)*	Standard deviation on strain (10^{-5})	Standard deviation on stress (*MPa*)	Computed Loading *(N)*
0	2.75	3.65	–
50	1.19	1. 61	51.6

It can also be observed in Table 1 that slightly worse results are obtained for 0N than for 50N. The origin of this feature is not totally clear yet. A possible explanation could be that random and systematic DIC errors are larger for very small displacements (<0.1pixel) than for every other sub-pixel displacement [15]. One can also not completely rule out possible tiny specimen motions during the Laue measurements at 0N; the specimen was small and difficult to maintain fixed under stress free conditions during the scan.

In figure 5(b), we report results obtained by [20] with the standard method described above. The associated standard deviation on strain is ~ 4.5×10^{-5}. It is clear that the new Laue- DIC approach proposed in this paper provides a significant improvement of stress and strain accuracy.

6. Conclusion

In this work, we have proposed a new Laue-DIC method based on the coupling between white beam Laue microdiffraction and DIC techniques. The method is suitable to determine Laue spot motion field between two different deformation states, *e.g.* within a heterogeneously deformed crystal, and to deduce the associated increment of local elastic strain (and related local stress) and lattice rotation, with micrometer spatial resolution.

The procedure can be decomposed into three steps:

- First, Laue pattern is indexed from the known structure of the crystal, *e.g.* thanks to the LaueTools software, and the orientation and strain of the crystal in the non-deformed configuration can be derived within uncertainties associated to the standard treatment method.
- Next, DIC technique is used to determine the spot motion field on the detector, with high accuracy.
- Finally, an identification method is used to evaluate the mechanical transformation between two loadings states, and then to compute the increment of elastic strain and stress.

With this approach, local stresses are estimated with high accuracy: the standard deviation of the error is found to be about 3MPa in the considered Si single crystal deformed under four point bending. A more detailed comparison between the experimental and theoretical strain profiles in the Si wafer will be presented elsewhere, that will include Finite Element simulations and measured profiles for all strain and rotation components. Thanks to the sub-micron size of the X-ray beam and the possibility to perform sub-micron movements of the sample under the detector, heterogeneities in the stress field can be detected with a micrometric resolution. The method can thus be applied for generating intragranular stress field maps in deformed polycrystals. Note also that there is still room to improve the new Laue-DIC method a step further, *e.g.* by weighting Laue spots according to their intensity or intensity gradient during the identification stage.

Acknowledgements

Authors are very grateful to P. Goudeau (Inst. Pprime, France), G. Geandier (Inst. J. Lamour, France) and J.L. Béchade (CEA-Saclay, France) for stimulating discussions on Laue microdiffraction analyses and their help during very first experiments. Financial supports from the Fédération Francilienne de Mécanique (F2Mmsp, CNRS FR2609) and from the French agency ANR (project # ANR-11-BS09-030-MICROSTRESS) are acknowledged.

References

[1] Shenoy GK, Vicarro PJ, Mills DM. Characteritics of the 7-GeV Advanced Photon Source: A Guide for Users ANL-88-9. Argonne National Laboratory, Argonne, IL; 1988.

[2] Mills DM. Third-Generation Hard X-ray Synchrotron Radiation Sources: Source Properties, Optics and Experimental Techniques. In: John Wiley and Sons, editors; 2002.

[3] Buras B, Tazzari S. European synchrotron radiation facility – Report of the ESRP. Cern LEP Div., Geneva, Switzerland; 1984.

[4] Barabash R, Ice GE, Larson BC, Pharr GM, Chung KS, Yang W. White microbeam diffraction from distorted crystals. *Applied Physics Lettters* 2001; **79**(6):749–51.

[5] Tamura N, MacDowell AA, Celestre RS, Padmore HA, Valek B, Bravman JC, Spolenak R, Brown WL, Marieb T, Fujimoto H, Batterman BW, Patel JR. High Spatial resolution grain orientationand strin maping in thin films using polychromatic submicron x-ray diffraction. *Applied Physics Lettters* 2002; **80**(19):1–3.

[6] Mughrabi H, Ungár T. Close up on crystal plasticit: A novel X-ray diffraction technique opens way to investigate deformation-induced dislocation microstructures with submicrometre resolution. *Nature Materials* 2006; **5**:602–10.

[7] http://xraysweb.lbl.gov/microdif/user_resources.htm, https://sites.google.com/a/lbl.gov/bl12-3-2/

[8] Chung JS, Ice GE. *Journal of Applied Physics* 1999; **86**(52):49–55.

[9] Tamura N, Celestre RS, MacDowell AA, Padmore HA, Spolenak R et al. In Papers from the 12th National Synchrotron Radiation Instrumentation Conference, volume 73, 1369–72 (AIP, Madison, Wisconsin (USA)), 2002.

[10] http://sourceforge.net/projects/lauetools/

[11] Hofmann F, Korsunsky AM. Micro-beam Laue Diffraction: An Error Analysis. Proceedings of the *Euromech 2010* Colloquium on metal fatigue, Ecole Polytechnique, Paris 2010

[12] Sutton MA, Orteu JJ, Schreier HW. Image Correlation for Shape, Motion and Deformation Measurements. In: Springer, editors; 2009.

[13] Castelnau O, Drakopoulos M, Schroer C, Snigireva I, Snigirev A, Ungar T, Dislocation density analysis in single grains of steel by X-ray scanning microdiffraction, *Nucl. Instr. and Meth. A*, **467-468**, P. 1245-1248, 2001.

[14] Ungàr T, Castelnau O, Ribàrik G, Drakopoulos M, Béchade JL et al. Grain to grain activity in cold rolled Zr determined by X-ray microdiffraction line profile analysis, *Acta Mater.*, **55**, p.1117-1127, 2007.

[15] Bornert M, Brémand F, Doumalin P, Dupré JC, Fazzini M, Grédiac M et al. Assessment of Digital Image Correlation Measurement Errors: Methodology and Results. *Experimental Mechanics* 2008.

[16] Sutton MA, Wolters WJ, Peters WH, Ranson WF, McNeil SR. Determination of displacements using an improved digital correlation method. *Image vision Comput* 1983;1(3):133–9.

[17] Sutton MA, Wolters WJ, Peters WH, Ranson WF, McNeil SR. Application of an optimised digital image correlation method to planar deformation analysis. *Image vision Comput* 1986;4(3):143–51.

[18] Bornert M, Valès F, Gharbi H, Nguyen Minh D. Multiscale Full-Field Strain Measurements for Micromechanical Investigations of the Hydromechanical Behaviour of Clayey Rocks. *Strain* 2010; **46**: 33–46.

[19] Doumalin P. Microextensométrie locale par corrélation d'images numériques; application aux études micromécaniques par microscopie électronique à balayage. PhD thesis 2000, École Polytechnique, Palaiseau, France.

[20] Hofmann F, DPhil thesis: Probing the Deformation of Ductile Polycrystals by Synchrotron X-ray Microdiffraction, University of Oxford, March 2011.